



## OPEN

## Influence of doping on charge carrier collection in normal and inverted geometry polymer:fullerene solar cells

George F. A. Dibb<sup>1,2,3</sup>, Mathis-Andreas Muth<sup>4,5</sup>, Thomas Kirchartz<sup>1,3</sup>, Sebastian Engmann<sup>6</sup>, Harald Hoppe<sup>6</sup>, Gerhard Gobsch<sup>6</sup>, Mukundan Thelakkat<sup>5</sup>, Nicolas Blouin<sup>4</sup>, Steve Tierney<sup>4</sup>, Miguel Carrasco-Orozco<sup>4</sup>, James R. Durrant<sup>2,3</sup> & Jenny Nelson<sup>1,3</sup>

<sup>1</sup>Department of Physics, Imperial College London, Exhibition Road, London, SW7 2AZ, United Kingdom, <sup>2</sup>Department of Chemistry, Imperial College London, Exhibition Road, London, SW7 2AZ, United Kingdom, <sup>3</sup>Centre for Plastic Electronics, Imperial College London, Exhibition Road, London, SW7 2AZ, United Kingdom, <sup>4</sup>Merck Chemicals Ltd., Chilworth Science Park, Southampton, SO16 7QD, United Kingdom, <sup>5</sup>Department of Macromolecular Chemistry I, Applied Functional Polymers, Universität Bayreuth, Universitätsstraße 30, 95440 Bayreuth, Germany, <sup>6</sup>Institute of Physics and Institute of Micro- and Nanotechnologies, Ilmenau University of Technology, 98693 Ilmenau, Germany.

Received  
22 July 2013

Accepted  
8 November 2013

Published  
26 November 2013

Correspondence and requests for materials should be addressed to J.N. (jenny.nelson@imperial.ac.uk)

While organic semiconductors used in polymer:fullerene photovoltaics are generally not intentionally doped, significant levels of unintentional doping have previously been reported in the literature. Here, we explain the differences in photocurrent collection between standard (transparent anode) and inverted (transparent cathode) low band-gap polymer:fullerene solar cells in terms of unintentional p-type doping. Using capacitance/voltage measurements, we find that the devices exhibit doping levels of order  $10^{16} \text{ cm}^{-3}$ , resulting in space-charge regions  $\sim 100 \text{ nm}$  thick at short circuit. As a result, low field regions form in devices thicker than  $100 \text{ nm}$ . Because more of the light is absorbed in the low field region in standard than in inverted architectures, the losses due to inefficient charge collection are greater in standard architectures. Using optical modelling, we show that the observed trends in photocurrent with device architecture and thickness can be explained if only charge carriers photogenerated in the depletion region contribute to the photocurrent.

The record power conversion efficiency (PCE) achieved by polymer:fullerene solar cells has increased considerably in the past 4 years to a record published value of 9.2%<sup>1</sup> for a single bulk heterojunction and efficiencies of 10.6% for tandem solar cells<sup>2</sup>. This is despite the fact that organic semiconductors are known to be both structurally and electronically disordered, have lower dielectric constants inhibiting separation of the photogenerated excitonic species and have charge carrier mobilities orders of magnitude lower than inorganic semiconductors.

Whilst charge mobilities are low in organic semiconductors and collection losses have been shown to limit the fill factor ( $FF$ )<sup>3–5</sup> and short circuit current density ( $J_{SC}$ )<sup>6–10</sup> of certain devices, low mobilities do not necessarily prevent devices from performing efficiently. However the lower charge mobilities and diffusion coefficients in organic semiconductors do mean that diffusion alone is insufficient for charge carrier collection and drift must account for a large proportion of the generated photocurrent. Additionally, polymer:fullerene solar cells are not intentionally doped like their inorganic counterparts or like many small molecule solar cells<sup>11</sup> and therefore rely on selective contacts and the difference in work function between electrodes for efficient charge collection. However, several studies have found evidence for unintentional doping<sup>12–19</sup> and discussed the consequences for device behaviour<sup>6,20–30</sup>. Whilst the origin of this doping is unclear<sup>15</sup>, its effects on photovoltaic performance can be substantial; however many recent analyses of device performance neglect doping<sup>8,31–33</sup> despite the fact that the influence of doping and the electric field on charge carrier collection is well known for a long time<sup>34</sup> and well-studied for instance in the field of quantum dot photovoltaics<sup>35,36</sup>.

In this paper, we address the importance of non-uniform electric fields within organic photovoltaic devices and the impact of this upon device performance. The field distribution in such devices is often described in terms of a metal-insulator-metal model, where charge on the metallic electrodes results in the generation of relatively uniform electric fields in the device. However, non-uniform electric fields will develop when there is an excess



of one polarity of charge carrier within the active layer of a device. Such net space-charge can be caused by electronic or chemical doping<sup>6,25</sup> or unequal charge carrier mobilities<sup>37</sup>. For sufficiently high space charge densities in sufficiently thick devices, the active layer thickness exceeds the width of the depletion region, leaving a field-free, neutral region through which minority carriers must diffuse. In the depletion approximation the width of the depletion region  $w$  in a doped semiconductor device at an applied bias  $V$  is given by

$$w = \sqrt{\frac{2\epsilon_r\epsilon_0(V_{BI} - V)}{qN_A}} \quad (1)$$

where  $\epsilon_0$  is the dielectric constant of the vacuum,  $\epsilon_r$  is the relative dielectric permittivity of the semiconducting material,  $V_{BI}$  is the built-in voltage,  $q$  is the elementary charge and  $N_A$  is the net doping density. For the typical mobilities, charge carrier lifetimes and thicknesses of organic solar cells, charge collection by diffusion in a region of low electric field is less efficient than drift-driven collection in a space charge region. This has been shown before by numerical simulations<sup>38</sup> and can be rationalized by considering typical drift and diffusion lengths. If we take a simple example of a device with thickness  $d = 100$  nm and built-in voltage  $V_{BI} = 1$  V, then a mobility-lifetime product  $\mu\tau = 10^{-10}$  cm<sup>2</sup>/V would lead to a drift length  $L_{dr} = \mu\tau V_{BI}/d = 100$  nm at short circuit, such that  $1 - e^{-1} = 63\%$  of charges would be collected according to the Hecht-equation<sup>39</sup>. At the same time, the diffusion length for the same mobility-lifetime product, would only be  $L_{diff} = \sqrt{\mu\tau kT/q} = 16$  nm.

Charge collection from the neutral region is further inhibited by the fact that the lifetimes of minority carriers scale inversely with the density of majority carriers. For a p-type semiconductor, the higher density of holes in the neutral region than in the depletion region results in a reduction in electron lifetime  $\tau$  and hence in the  $\mu\tau$ -product within the neutral region. Consequently, the diffusion length in the neutral region is even smaller than would be expected on the basis of the  $\mu\tau$ -product for the space charge region. In the case of a p-type device the depletion region (high electric field) forms at the cathode and the neutral region (low electric field) at the anode, meaning that minority carriers generated near the anode are harder to collect than those generated near the cathode.

## Results

As a model system to investigate the effects of space-charge we consider standard (transparent anode) and inverted (transparent cathode) bulk heterojunction solar cells made from a low band gap conjugated polymer poly[2,6[4,8-bis(2-ethyl-hexyl)benzo[1,2-b;4,5-b']dithiophene-co-2,5-thiophene-co-4,7[5,6-bis(octyloxy-benzo[1,2,5]thiadiazole)-co-2,5-thiophene] (PBDTTBTZT)<sup>40</sup>, whose structure is shown in Figure 1, blended with [6,6]-phenyl-C<sub>71</sub>-butyric acid methyl ester (PC<sub>71</sub>BM). The polymer PBDTTBTZT was selected as a promising donor polymer that has previously exhibited good device efficiencies when blended with PCBM<sup>40</sup>, and which can easily be fabricated with a variety of layer thicknesses due

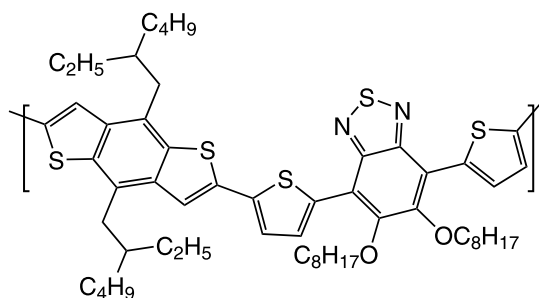
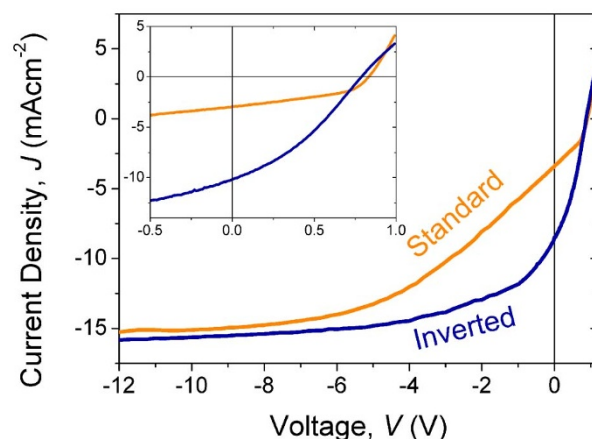


**Figure 1** | PBDTTBTZT Structure.

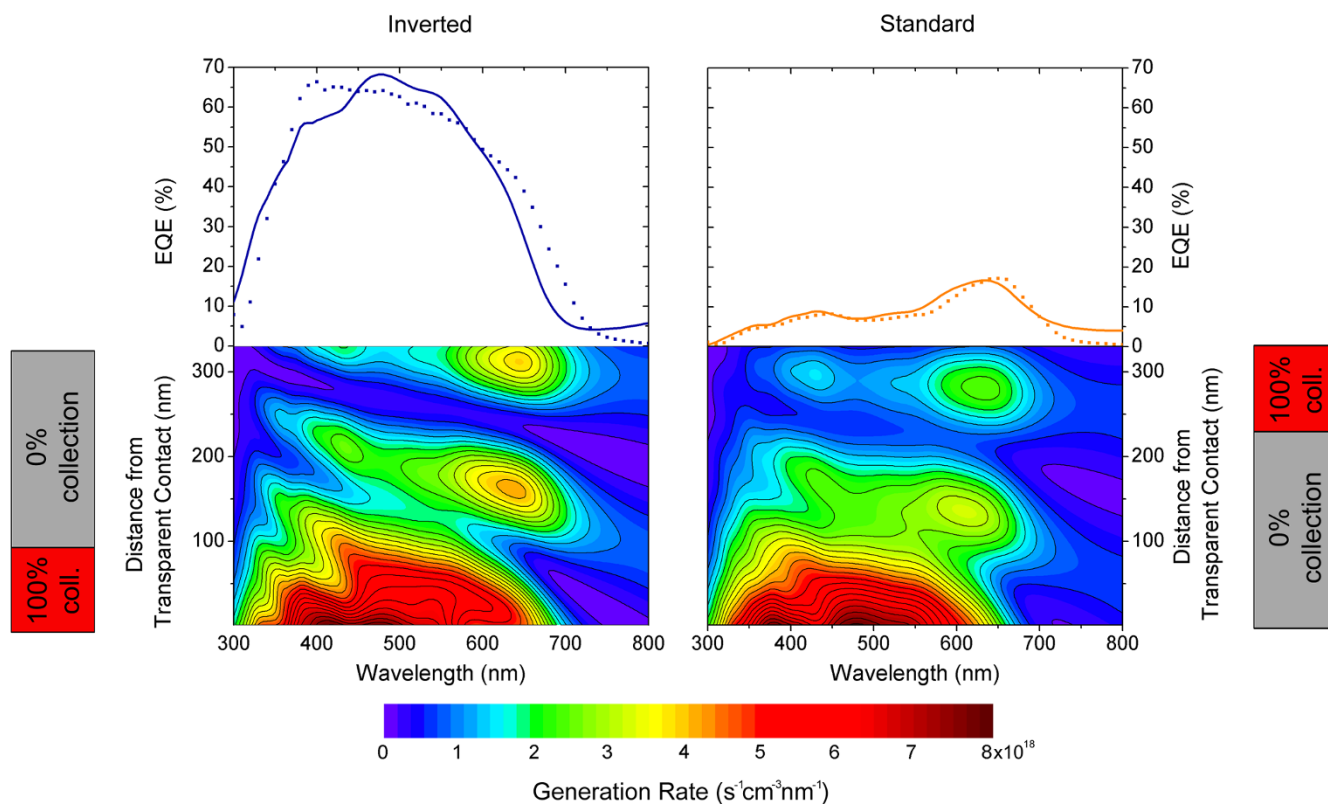
to its versatility and ease of blade coating. Devices with the layer structure ITO/PEDOT:PSS/PBDTTBTZT:PC<sub>71</sub>BM/Ca/Al (standard) and ITO/ZnO/PBDTTBTZT:PC<sub>71</sub>BM/PEDOT:PSS/Ag (inverted), both with an active layer thicknesses of 330 nm, were studied with light and dark current density-voltage ( $J$ - $V$ ) and external quantum efficiency (EQE) measurements.

Figure 2 shows the corrected photocurrent curves of standard and inverted devices measured into far reverse bias, calculated by subtracting the  $J$ - $V$  curve obtained in the dark from that under 1 sun illumination. The inset shows the  $J$ - $V$  curves of both devices in the power generating quadrant. The  $J$ - $V$  curves exhibit large differences in the short circuit current density ( $J_{SC}$ ) and the fill factor ( $FF$ ) due to a large linear region in the  $J$ - $V$  curve of the standard device between  $-6$  and  $+0.7$  V.  $J$ - $V$  curves of devices fabricated from the same solution but with thinner active layers of approximately 100 nm are shown in Figure S1 in the Supporting Information. In contrast to the results obtained on the thick devices, these devices show a much smaller discrepancy in  $J_{SC}$  and  $FF$  between normal and inverted structures. Additionally, external quantum efficiency spectra of the thick devices shown as points in the EQE plots of Figure 3 indicate considerable differences in both the magnitude and the wavelength dependence of photocurrent generation, whilst the absorption spectra of the completed devices without metal contacts (Supp. Inf. Figure S2) indicate that the absorption of photons is almost identical. This indicates a wavelength dependence of either charge generation or collection efficiency.

The linear region in the  $J$ - $V$  curve of the standard device, which limits the  $FF$  and  $J_{SC}$  of the solar cell, is characteristic of charge transport that is limited by carrier diffusion in that voltage region<sup>25</sup>. As these are relatively thick devices it is possible that a space-charge induced neutral region is limiting the efficient extraction of charge carriers. We utilised capacitance-voltage measurements in the dark to determine the degree to which a depletion region is present in the active layer. Capacitance-voltage measurements are an established technique used to determine the doping density of a semiconductor<sup>6,19,29,38,41–43</sup>. The width of the space-charge region is probed by a variation of the DC voltage and is detected by measuring the capacitance of the device as a function of the DC voltage. The capacitance is proportional to  $(V - V_{BI})^{-1/2}$ . Thus, we analyzed the data using the Mott-Schottky analysis leading to dopant densities of  $N_A \approx 4 \times 10^{16}$  cm<sup>-3</sup> of an excess of positive carriers in both devices (shown in SI Fig S4)<sup>41</sup>. This is a relatively high dopant concentration and thus space-charge effects will be playing a part in carrier extraction. The capacitance voltage measurements are performed and analysed in



**Figure 2** | Corrected photocurrents for both the standard and inverted PBDTTBTZT:PC<sub>71</sub>BM devices with active layer thicknesses of 330 nm, measured to far reverse biases under 1 sun illumination. Inset shows the power generating quadrant of the current density – voltage ( $J$ - $V$ ) curves measured under 1 sun illumination for the same devices.



**Figure 3** | Top panels: Comparison of experimentally measured external quantum efficiency spectra (dotted lines) for inverted (left) and standard (right) architecture PBDTTBTZT:PC<sub>71</sub>BM devices, with simulated EQE spectra (full lines) obtained using the simple model (see text). Bottom panels: spectral charge generation rate as a function of depth calculated using a transfer matrix model of photon absorption. In this figure the light enters the device from the bottom of the figure (0 nm on the y-axis). For each device architecture, the red block indicates the part of the active layer in which generated charges can be collected at short circuit, according to the model used here. Only charges generated within these regions contribute to the simulated EQE.

the dark under reverse and low forward bias. Under these conditions, there are not many charge carriers injected into the device and no excess carriers are created optically. Therefore build-up of space charge due to asymmetric mobilities does not affect the capacitance measurements and we can be sure that the Mott-Schottky type behaviour of the capacitance must be due to doping. Using equation 1 and the depletion approximation, we calculate that the resulting depletion region must extend approximately 100 nm from the cathode in both devices ( $V_{BI} = 0.8$  V,  $\epsilon_r = 4.0$ ). We validate this calculation by comparing the results with a more complex drift-diffusion simulation as published elsewhere<sup>44,45</sup>, described more fully in the supporting information (Figure S5). We additionally note that the electron and hole mobilities derived from the fitting of the drift-diffusion model, are of the same order as those measured using space-charge limited current by Muth et. al. on the same polymer system<sup>40</sup>.

To understand how the reduced collection in the neutral zone impacts the device performance it is essential to know where in the active layer charges are being generated. Photon absorption within thin multilayered structures such as organic solar cells is influenced by interference effects and is not trivial to describe. In such structures, the spatially and spectrally resolved generation rate can be calculated from the complex optical functions of the materials using the transfer matrix method (TMM)<sup>46–48</sup>. In this work the complex refractive index of the PBDTTBTZT:PC<sub>71</sub>BM blend was obtained via spectroscopic ellipsometry (see experimental section and SI). Figure 3 shows contour plots of the optical generation rate, or the rate of exciton generation per unit thickness and wavelength, in the active layer of both standard and inverted devices. The photon absorption profiles are very similar in both device architectures,

and both the standard and the inverted device absorb the majority of incident photons.

To understand the impact of the depletion region upon photocurrent generation we first approximate the band-diagram of the device, shown in figure 4, as two distinct regions. The region on the left of the figure is the neutral region of the device where charge transport is via diffusion and charge collection is relatively inefficient. While the right hand region represents the depletion region with a constant electric field where charge collection is relatively efficient<sup>25</sup>. We approximate charge collection as a step-function, with 0% collection in the neutral region and 100% collection in the depletion region. We also assume short exciton diffusion lengths, thus charges are generated very close to where the respective photon is absorbed.

Applying this charge collection approximation to the photon absorption profiles we can simulate the device EQEs. As can be seen in figure 3, in both the standard and inverted devices the majority of photo-absorption occurs within the first 100 nm of the active layer, at least within the wavelength range of 350–600 nm where the PBDTTBTZT:PC<sub>71</sub>BM blend absorbs strongly. However red light of wavelength  $\lambda \approx 650$  nm is not absorbed strongly but penetrates the device, reflecting from the metal electrode and forming interference fringes. The EQE spectra reconstructed from the absorption profiles and the simple collection model are shown as solid lines in figure 3. Clearly for both devices the modelled EQE spectra are similar to the experimentally measured ones, capturing the main features in the spectra. In the inverted device most of the absorption assigned to the main broad band of PBDTTBTZT:PC<sub>71</sub>BM blend absorption (350–650 nm) occurs in the collection region, thus the EQE of this device closely resembles the absorption spectrum. In the

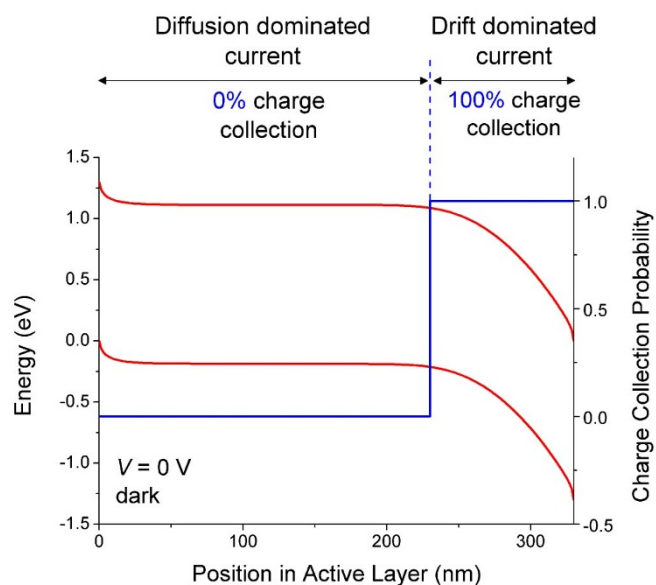


**Figure 4** | A band diagram at short circuit in the dark, calculated from a drift-diffusion simulation of a device with  $N_A = 4 \times 10^{16} \text{ cm}^{-3}$ . The p-type doping causes non-uniform electric field within the active layer of a thick device (red). The solid blue line indicates the simple step-function charge collection function used in this model.

standard device, the majority of this strong photon absorption occurs in the neutral region and therefore it doesn't contribute to photocurrent. However absorption due to the interference peak around 650 nm does occur in the collection region, causing the EQE to peak at 650 nm.

Equation 1 determines how the size of the depletion region varies with voltage, showing that as a device is swept into reverse bias more and more of the device will become depleted. Thus by integrating the photon absorption in collection regions of varying size, and relating that to the bias required to achieve that depletion region, a recreation of the charge collection as a function of voltage can be performed; in other words the  $J$ - $V$  curve can be simulated. The results of these simulations for the inverted and standard devices are shown in the supporting information Figure S6, showing a remarkable similarity with the fill factors and unusually shaped corrected photocurrent curves shown in Figure 2. Additionally the total number of photons absorbed in the inverted device is slightly higher than in the standard architecture, consistent with the slightly higher corrected photocurrent observed in the inverted device under far reverse bias (Figure 2) where the entire device will be depleted.

The agreement between the measured EQE spectra and our simple model demonstrates that photocurrent generation is indeed limited by the inability to collect charges from the neutral region. This also explains the difference in the  $J_{SC}$  between standard and inverted devices. Furthermore, the similar open circuit voltage ( $V_{OC}$ ) values for the standard and inverted devices can be explained by the fact that under open-circuit conditions both devices are in effective flat-band conditions and the differences in electric field distribution disappear.

Evidently device thickness strongly impacts charge collection, particularly when the device thickness extends beyond the depletion region thickness. Several other additional factors affect the measured photocurrent in addition to space-charge related collection issues, such as the donor:acceptor blend morphology, the presence of direct percolation pathways and the distribution of energetic trap states. We now study the thickness dependence of charge collection on the same polymer:fullerene system as above. The devices for this study differ from the previous set only in the solvent used, which is ortho-dichlorobenzene rather than chloroform as used above. We cannot

rule out any effect of solvent on charge collection via an effect on blend microstructure. However, we show below that the thickness dependence of PBDTTBTZT:PC<sub>71</sub>BM device performance can be explained completely by space-charge effects using the same model as above. Figure 5a shows the  $J$ - $V$  characteristics of a series of standard architecture PBDTTBTZT:PC<sub>71</sub>BM devices fabricated from ortho-dichlorobenzene solution with thicknesses from 80–400 nm. Devices made using this solvent appear to have slightly higher efficiencies (see table of device parameters in SI), thus the 310 nm thick device performs slightly better than the standard architecture 330 nm device studied above. Whilst the  $V_{OC}$  for these devices is relatively constant with active layer thickness, and the fill factor is reduced at higher thicknesses, the biggest limit to power conversion efficiency in the thicker devices is their considerably reduced  $J_{SC}$ <sup>49</sup>. Due to interference effects, the number of photons absorbed as a function of cell thickness increases monotonically, yet cannot be described by a simple function<sup>50,51</sup>. The line in figure 5b shows the thickness dependence of the total photon absorption within the active layer in comparison with the measured  $J_{SC}$ . The substantial deviation between the potential  $J_{SC}$  due to the simulated absorption profiles and the actually measured  $J_{SC}$  shows that additional loss processes must reduce the short circuit current at high thicknesses. This reduction in  $J_{SC}$  is accompanied by a significant reduction and wavelength shift in the simulated EQE of the devices as shown below.

The changes in photon absorption between devices of different thicknesses are clearly shown in the contour plots of absorption in the active layer shown in figure 6. We employ the same simple device model as above assuming a depletion depth of 100 nm, and that all charges resulting from photon absorption within this depth of the cathode are collected, as shown by the red bars in Figure 6. We can again predict the EQE spectra, and thus the short-circuit current densities, and compare those to the experimentally measured EQE spectra shown in Figure 7a. The thinnest device having an active layer thickness of 80 nm is fully depleted and all photogenerated charges are collected; the device with thickness of 130 nm will only be marginally affected. However, the thicker devices all see large changes in charge collection as in the standard architecture only charges close to the back contact are collected. Figure 7b shows the EQE spectra predicted by the collection model from photon absorption profiles shown in figure 6, where charge collection is limited to within 100 nm of the cathode. Again the simulated spectra closely match the experimental EQE spectra and the trend in relative height of absorption peaks as thickness increases. This demonstrates that this model of collection can be successfully applied to optimised devices and those with thinner active layers, as well as those where only a portion of the thickness is depleted.

Whilst the EQE simulation for the thinner devices is very good, the magnitude of the EQE spectra, and consequently the predicted  $J_{SC}$  calculated by integrating the EQE, are underestimated by the simple collection model in the thicker devices. This shows that with thicker active layers, the BHJs fabricated with oDCB collect charges more efficiently, and that perhaps the improved performance of the oDCB devices is due to increased charge collection from within the neutral region of the device. Additionally it is possible that due to differences in the imbalance between electron and hole mobilities, or the electronic doping concentration, the size of the depletion region in these thick devices is different to that of devices fabricated with chloroform, however in this case the shape of the EQE would be expected to change, not just its magnitude.

## Discussion

We have shown above that photocurrent generation in PBDTTBTZT:PCBM solar cells can be explained by a simple model of carrier collection limited by the extent of the space charge region and its position relative to the transparent electrode. Here, we address some of the assumptions underlying this simple model and the possible

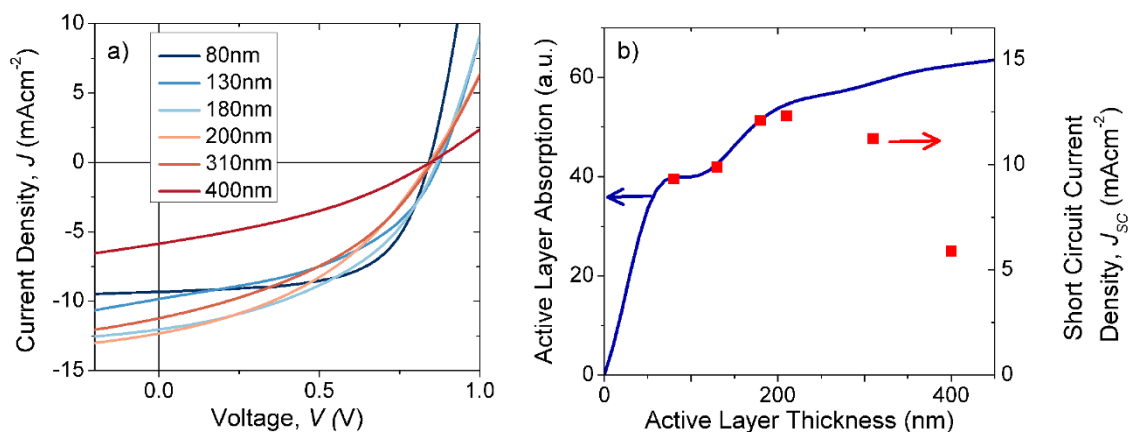


**Figure 5** | (a)  $J$ - $V$  curves for six standard architecture PBDTTBTZT:PC<sub>71</sub>BM devices with different active layer thicknesses, measured under 1 sun illumination and (b) a plot showing the variation with active layer thicknesses of photon absorption from transfer matrix modelling (line) and short circuit current density from experiments (points).

origin of the doping effect. The assumptions that we made during the modelling of charge collection, i.e. separating the device into two regions with 0% and 100% collection, are validated by the similarities between the EQE spectra obtained using a numerical drift-diffusion model (shown in SI) and those in figure 3. The drift-diffusion model takes into account the precise form of the spatially varying electric field and resulting variations in recombination caused by the varying charge density in the device, and such a model gives very similar EQE spectra to those calculated using the simple step-function model. As with one-dimensional drift-diffusion modelling the simple collection model described here doesn't take into account the BHJ structure of polymer:fullerene solar cells or differences in microstructure throughout devices, however a close match with experimental results

is achieved with the use of no fitting parameters. We consider the close agreement between the experimental data, the results of the simple model and the results of complex numerical simulations to serve as a verification of the use of the simple model in understanding the effects of doping upon charge collection.

The dopant concentration ( $\sim 4 \times 10^{16} \text{ cm}^{-3}$ ) measured in these devices is relatively high, affecting the collection of charges in devices that are made thick enough to absorb at the second absorption maximum. Consequently the doping of the active layer prevents devices fabricated from a blend of PBDTTBTZT:PC<sub>71</sub>BM from reaching the maximum obtainable  $J_{\text{SC}}$ . Were the dopant density to be an order of magnitude lower, the depletion region would more than triple in width according to Eq. (1). Therefore the electric field would be

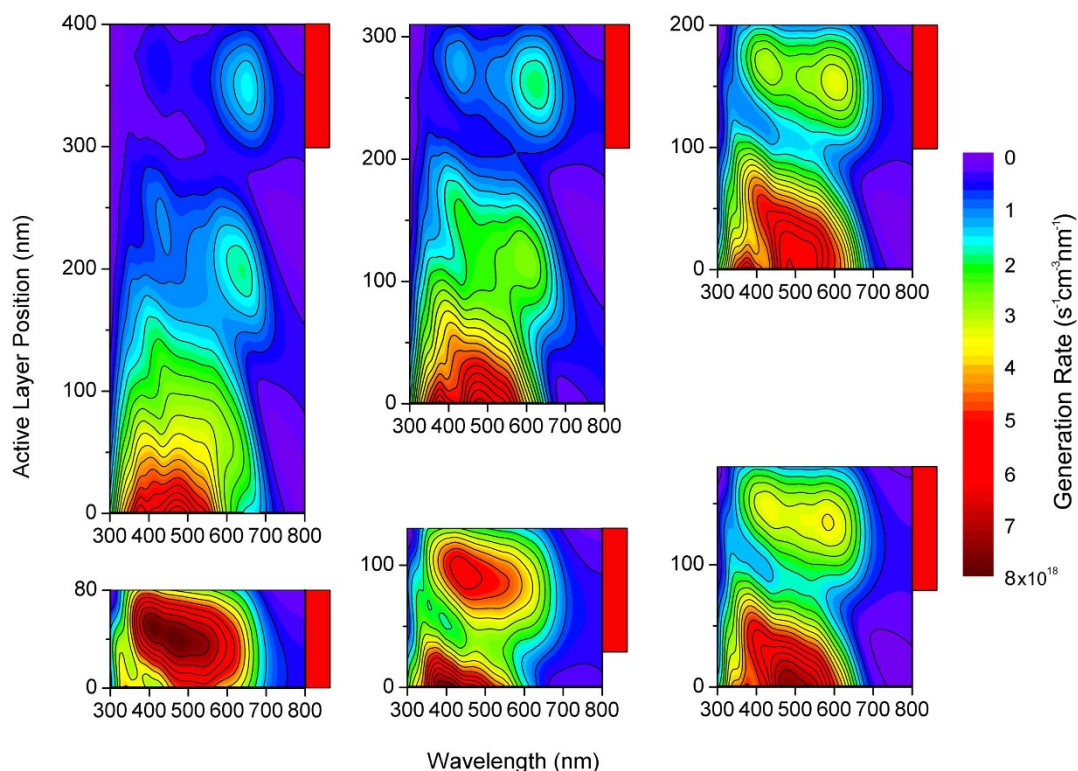


**Figure 6** | Contour plots showing the photon absorption (or charge generation) rates throughout the active layer of the six different standard architecture PBDTTBTZT:PC<sub>71</sub>BM devices (thicknesses of 80, 130, 180, 200, 310 & 400 nm). The red bar alongside each one indicates the width of the depletion region (100 nm) from the cathode in which charges can be efficiently collected.

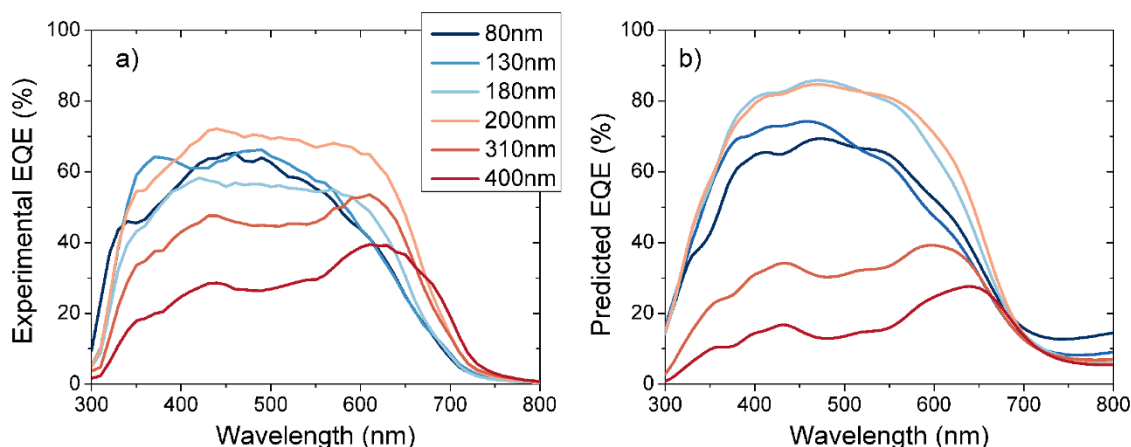


**Figure 7** | plots of external quantum efficiency spectra for standard architecture PBDTTBTZT:PC<sub>71</sub>BM devices with different active layer thicknesses from experiment (a) and from modelling of charge carrier collection (b).

uniformly distributed even in a device with an active layer thickness greater than 300 nm. Figure 5 indicates that were the charge collection in the 400 nm thick device efficient throughout the device then the  $J_{SC}$  could be a significant 20% higher than the actual maximum  $J_{SC}$  measured in the 210 nm thick device. This clearly neglects the other factors affecting collection such as changes in mobility and charge carrier lifetime, however it indicates the advantages of reducing dopant density. Given the importance of device thickness in optimising photocurrent generation, this indicates that material doping may be a critical, but hitherto largely unconsidered, parameter in achieving efficient OPV device performance.

Currently the cause of electronic doping of the active layer is unclear, although several potential candidates have been identified. Unintended or incomplete synthetic products have been shown to significantly reduce device efficiency and to be very difficult to detect<sup>42,52</sup>. Whether these could dope a device depends on the specific molecular properties. Additionally, synthetic routes for conjugated polymers typically involve the use of metallic catalysts, which results in low concentrations of metal atoms in the final synthetic product, as methods for subsequently removing the catalyst are imperfect<sup>53,54</sup>. Finally, the presence of unwanted oxygen, either in its diatomic or radical state, has been shown to form trap states in the semiconductor density of states of the blend<sup>55–57</sup>, thus altering device performance. It has been suggested that this could additionally electronically dope the blend material<sup>12,14,16,58</sup>. Evidently there are uncertainties around the actual cause of the electronic doping, however we have shown here that this is a significant effect that must be considered and should be the subject of further study. Additionally evidence would suggest that almost all organic semiconductors are doped to a certain extent making a true comparison of doped vs. undoped devices impossible.

We propose a model consisting of consideration of the depletion region width, and then a simple step-function collection model with collection probabilities of 100% and 0% to explain device performance for a solar cell with space-charge effects resulting from moderate electronic doping, although this could apply equally well to devices limited by unequal charge mobilities. Furthermore we propose that large discrepancies in the EQE of devices fabricated with the same blend but in inverted and standard architectures are indicators that the device is being limited by poor charge collection caused by non-uniform electric fields in the device. As long as the dopant concentration is known this simple model can be applied to understand the charge collection losses limiting the device operation.

To conclude, we have shown in this paper that non-uniform electric fields caused by space-charge accumulation can cause significant collection losses in organic solar cells, changing the EQE of the device

and severely limiting the device  $J_{SC}$ . This field non-uniformity accounts for the large discrepancy between the performance of standard and inverted devices with the same thickness and for the evident charge collection losses and low  $J_{sc}$ s in thick devices.

## Methods

Solar cell devices were fabricated in both standard (ITO/PEDOT:PSS/PBDTTBTZT:PC<sub>71</sub>BM/Ca/Al) and inverted (ITO/ZnO/PBDTTBTZT:PC<sub>71</sub>BM/PEDOT:PSS/Ag) architectures, as described by Muth et al.<sup>40</sup>. Briefly, these were made by blade-coating a PBDTTBTZT:PC<sub>71</sub>BM solution in CHCl<sub>3</sub>, this technique allows for greater control of the active layer thickness than spin-coating and these devices were intentionally fabricated with thick active layers of 330 nm in both devices. Another series of PBDTTBTZT:PC<sub>71</sub>BM devices were fabricated, this time blade coated from a dichlorobenzene (oDCB) solution, at six different thicknesses; 80, 130, 180, 210, 310 and 400 nm thick active layers. These devices were in the standard architecture thus the layer stack was ITO/PEDOT:PSS/PBDTTBTZT:PC<sub>71</sub>BM/Ca/Al. Information of spectroscopic ellipsometry can be found in the supporting information.

1. He, Z. C. *et al.* Enhanced power-conversion efficiency in polymer solar cells using an inverted device structure. *Nat. Photon.* **6**, 591–595 (2012).
2. You, J. *et al.* A polymer tandem solar cell with 10.6% power conversion efficiency. *Nat Commun* **4**, 1446 (2013).
3. Tress, W. *et al.* Correlation of Absorption Profile and Fill Factor in Organic Solar Cells: The Role of Mobility Imbalance. *Adv. En. Mat.* **3**, 631–638 (2013).
4. Proctor, C. M., Kim, C., Neher, D. & Nguyen, T.-Q. Nongeminate Recombination and Charge Transport Limitations in Diketopyrrolopyrrole-Based Solution-Processed Small Molecule Solar Cells. *Adv. Funct. Mater.* **23**, 3584–3594 (2013).
5. Savoie, B. M., Movaghar, B., Marks, T. J. & Ratner, M. A. Simple Analytic Description of Collection Efficiency in Organic Photovoltaics. *J. Phys. Chem. Lett.* **4**, 704–709 (2013).
6. Kirchartz, T., Agostinelli, T., Campoy-Quiles, M., Gong, W. & Nelson, J. Understanding the Thickness-Dependent Performance of Organic Bulk Heterojunction Solar Cells: The Influence of Mobility, Lifetime, and Space Charge. *J. Phys. Chem. Lett.* **3**, 3470–3475 (2012).
7. Azimi, H., Senes, A., Scharber, M. C., Hingerl, K. & Brabec, C. J. Charge Transport and Recombination in Low-Bandgap Bulk Heterojunction Solar Cell using Bis-adduct Fullerene. *Adv. En. Mat.* **1**, 1162–1168 (2011).
8. Tumbleston, J. R., Liu, Y. C., Samulski, E. T. & Lopez, R. Interplay between Bimolecular Recombination and Carrier Transport Distances in Bulk Heterojunction Organic Solar Cells. *Adv. En. Mat.* **2**, 477–486 (2012).
9. Koster, L. J., Kemerink, M., Wienk, M. M., Maturrova, K. & Janssen, R. A. Quantifying bimolecular recombination losses in organic bulk heterojunction solar cells. *Adv Mater* **23**, 1670–1674 (2011).
10. Dibb, G. F. A., Jamieson, F. C., Maurano, A., Nelson, J. & Durrant, J. R. Limits on the Fill Factor in Organic Photovoltaics: Distinguishing Nongeminate and Geminate Recombination Mechanisms. *J. Phys. Chem. Lett.* 803–808 (2013).
11. Walzer, K., Maennig, B., Pfeiffer, M. & Leo, K. Highly Efficient Organic Devices Based on Electrically Doped Transport Layers. *Chem. Rev.* **107**, 1233–1271 (2007).
12. Luer, L. *et al.* Oxygen-induced quenching of photoexcited states in polythiophene films. *Org. Electron.* **5**, 83–89 (2004).
13. Liu, A. *et al.* Control of Electric Field Strength and Orientation at the Donor–Acceptor Interface in Organic Solar Cells. *Adv. Mater.* **20**, 1065–1070 (2008).



14. Hintz, H., Peisert, H., Egelhaaf, H. J. & Chassé, T. Reversible and Irreversible Light-Induced p-Doping of P3HT by Oxygen Studied by Photoelectron Spectroscopy (XPS/UPS). *J. Phys. Chem. C* **115**, 13373–13376 (2011).
15. Liang, Z. & Gregg, B. A. Compensating Poly(3-hexylthiophene) Reveals Its Doping Density and Its Strong Exciton Quenching by Free Carriers. *Adv. Mater.* **24**, 3258–3262 (2012).
16. Schafferhans, J., Baumann, A., Wagenpfahl, A., Deibel, C. & Dyakonov, V. Oxygen doping of P3HT:PCBM blends: Influence on trap states, charge carrier mobility and solar cell performance. *Org. Electron.* **11**, 1693–1700 (2010).
17. Morfa, A. J., Nardes, A. M., Shaheen, S. E., Kopidakis, N. & van de Lagemaat, J. Time-of-Flight Studies of Electron-Collection Kinetics in Polymer:Fullerene Bulk-Heterojunction Solar Cells. *Adv. Funct. Mater.* **21**, 2580–2586 (2011).
18. Fabregat-Santiago, F., Garcia-Belmonte, G., Mora-Sero, I. & Bisquert, J. Characterization of nanostructured hybrid and organic solar cells by impedance spectroscopy. *PCCP* **13**, 9083–9118 (2011).
19. Guerrero, A. *et al.* How the Charge-Neutrality Level of Interface States Controls Energy Level Alignment in Cathode Contacts of Organic Bulk-Heterojunction Solar Cells. *ACS Nano* **6**, 3453–3460 (2012).
20. Chan, M. Y., Lai, S. L., Fung, M. K., Lee, C. S. & Lee, S. T. Doping-induced efficiency enhancement in organic photovoltaic devices. *Appl. Phys. Lett.* **90**, 023504 (2007).
21. Maennig, B. *et al.* Controlled p-type doping of polycrystalline and amorphous organic layers: Self-consistent description of conductivity and field-effect mobility by a microscopic percolation model. *Phys. Rev. B: Condens. Matter* **64**, 195208 (2001).
22. Chan, C. K., Zhao, W., Kahn, A. & Hill, I. G. Influence of chemical doping on the performance of organic photovoltaic cells. *Appl. Phys. Lett.* **94**, 203306 (2009).
23. Kao, P.-C., Chu, S.-Y., Huang, H.-H., Tseng, Z.-L. & Chen, Y.-C. Improved efficiency of organic photovoltaic cells using tris (8-hydroxy-quinoline) aluminum as a doping material. *Thin Solid Films* **517**, 5301–5304 (2009).
24. Kröger, M. *et al.* P-type doping of organic wide band gap materials by transition metal oxides: A case-study on Molybdenum trioxide. *Org. Electron.* **10**, 932–938 (2009).
25. Trukhanov, V. A., Bruevich, V. V. & Paraschuk, D. Y. Effect of doping on performance of organic solar cells. *Phys. Rev. B: Condens. Matter* **84**, 205318 (2011).
26. Olthof, S. *et al.* Ultralow Doping in Organic Semiconductors: Evidence of Trap Filling. *Phys. Rev. Lett.* **109**, 176601 (2012).
27. Lüssem, B., Riede, M. & Leo, K. Doping of organic semiconductors. *Phys. Status Solidi A* **210**, 9–43 (2013).
28. Pingel, P. & Neher, D. Comprehensive picture of p-type doping of P3HT with the molecular acceptor F<sub>4</sub>TCNQ. *Phys. Rev. B: Condens. Matter* **87**, 115209 (2013).
29. Bisquert, J. & Garcia-Belmonte, G. On Voltage, Photovoltage, and Photocurrent in Bulk Heterojunction Organic Solar Cells. *J. Phys. Chem. Lett.* **2**, 1950–1964 (2011).
30. Armin, A. *et al.* Doping-Induced Screening of the Built-in-Field in Organic Solar Cells: Effect on Charge Transport and Recombination. *Adv. En. Mat.* **3**, 321–327 (2013).
31. Min Nam, Y., Huh, J. & Ho Jo, W. Optimization of thickness and morphology of active layer for high performance of bulk-heterojunction organic solar cells. *Sol. Energy Mater. Sol. Cells* **94**, 1118–1124 (2010).
32. Street, R. A., Krakaris, A. & Cowan, S. R. Recombination Through Different Types of Localized States in Organic Solar Cells. *Adv. Funct. Mater.* **22**, 4608–4619 (2012).
33. Pandey, R. & Holmes, R. J. Characterizing the charge collection efficiency in bulk heterojunction organic photovoltaic cells. *Appl. Phys. Lett.* **100**, 083303 (2012).
34. Gärtner, W. Depletion-Layer Photoeffects in Semiconductors. *Phys. Rev.* **116**, 84–87 (1959).
35. Pattantyus-Abraham, A. G. *et al.* Depleted-Heterojunction Colloidal Quantum Dot Solar Cells. *ACS Nano* **4**, 3374–3380 (2010).
36. Luther, J. M. *et al.* Stability Assessment on a 3% Bilayer PbS/ZnO Quantum Dot Heterojunction Solar Cell. *Adv. Mater.* **22**, 3704–3707 (2010).
37. Mihailtchi, V. D., Wildeman, J. & Blom, P. W. M. Space-Charge Limited Photocurrent. *Phys. Rev. Lett.* **94**, 126602 (2005).
38. Kirchartz, T. *et al.* Sensitivity of the Mott–Schottky Analysis in Organic Solar Cells. *J. Phys. Chem. C* **116**, 7672–7680 (2012).
39. Crandall, R. S. Transport in hydrogenated amorphous silicon p-i-n solar cells. *J. Appl. Phys.* **53**, 3350–3352 (1982).
40. Muth, M.-A. *et al.* Influence of charge carrier mobility and morphology on solar cell parameters in devices of mono- and bis-fullerene adducts. *Nanotech.* **24**, 484001 (2013).
41. Khelifi, S. *et al.* Investigation of defects by admittance spectroscopy measurements in poly (3-hexylthiophene):(6,6)-phenyl C<sub>61</sub>-butyric acid methyl ester organic solar cells degraded under air exposure. *J. Appl. Phys.* **110**, 094509 (2011).
42. Troshin, P. A. *et al.* Impedance Measurements as a Simple Tool to Control the Quality of Conjugated Polymers Designed for Photovoltaic Applications. *Adv. Funct. Mater.* **20**, 4351–4357 (2010).
43. Garcia-Belmonte, G. *et al.* Charge carrier mobility and lifetime of organic bulk heterojunctions analyzed by impedance spectroscopy. *Org. Electron.* **9**, 847–851 (2008).
44. Kirchartz, T., Pieters, B. E., Kirkpatrick, J., Rau, U. & Nelson, J. Recombination via Tail States in Polythiophene:Fullerene Solar Cells. *Phys. Rev. B: Condens. Matter* **83**, 115209 (2011).
45. Kirchartz, T. & Nelson, J. Meaning of reaction orders in polymer: fullerene solar cells. *Phys. Rev. B: Condens. Matter* **86** (2012).
46. Katsidis, C. C. & Siapakas, D. I. General Transfer-Matrix Method for Optical Multilayer Systems with Coherent, Partially Coherent, and Incoherent Interference. *Appl. Opt.* **41**, 3978–3987 (2002).
47. Hoppe, H., Arnold, N., Meissner, D. & Sariciftci, N. S. Modeling of optical absorption in conjugated polymer/fullerene bulk-heterojunction plastic solar cells. *Thin Solid Films* **451–452**, 589–592 (2004).
48. Pettersson, L. A. A., Roman, L. S. & Inganas, O. Modeling photocurrent action spectra of photovoltaic devices based on organic thin films. *J. Appl. Phys.* **86**, 487–496 (1999).
49. Lenes, M., Koster, L. J. A., Mihailtchi, V. D. & Blom, P. W. M. Thickness dependence of the efficiency of polymer:fullerene bulk heterojunction solar cells. *Appl. Phys. Lett.* **88**, 243502 (2006).
50. Hoppe, H., Shokhovets, S. & Gobsch, G. Inverse relation between photocurrent and absorption layer thickness in polymer solar cells. *Phys. Status Solidi RRL* **1**, R40–R42 (2007).
51. Peet, J. *et al.* Bulk heterojunction solar cells with thick active layers and high fill factors enabled by a bithiophene-co-thiazolothiazole push-pull copolymer. *Appl. Phys. Lett.* **98**, 043301 (2011).
52. Leong, W. L. *et al.* Role of trace impurities in the photovoltaic performance of solution processed small-molecule bulk heterojunction solar cells. *Chem. Sci.* **3**, 2103–2109 (2012).
53. Dimitriev, O. P. Doping of Polyaniline by Transition-Metal Salts. *Macromolecules* **37**, 3388–3395 (2004).
54. Mityashin, A., Cheyns, D., Rand, B. P. & Heremans, P. Understanding metal doping for organic electron transport layers. *Appl. Phys. Lett.* **100**, 053305 (2012).
55. Street, R. A. & Davies, D. M. Kinetics of light induced defect creation in organic solar cells. *Appl. Phys. Lett.* **102**, 043305 (2013).
56. Nicolai, H. T. *et al.* Unification of trap-limited electron transport in semiconducting polymers. *Nat Mater* **11**, 882–887 (2012).
57. Maddalena, F., Meijer, E. J., Asadi, K., de Leeuw, D. M. & Blom, P. W. M. Doping kinetics of organic semiconductors investigated by field-effect transistors. *Appl. Phys. Lett.* **97**, 043302–043302–043303 (2010).
58. Kumar, P. & Gaur, A. Model for the J-V characteristics of degraded polymer solar cells. *J. Appl. Phys.* **113**, 094505 (2013).

## Acknowledgments

G.F.A.D. thanks Merck Chemicals Ltd. and the UK Engineering and Physical Sciences Research Council (EPSRC) for the award of a CASE studentship, J.N. thanks the Royal Society for the award of an Industrial Fellowship and EPSRC (EP/G031088, EP/J500021) for financial support, and T.K. acknowledges funding by an Imperial College Junior Research Fellowship. We are grateful to Mariano Campoy Quiles and Florent Deledalle for useful discussions.

## Author contributions

Polymer was designed and synthesised by N.B. under the guidance of S.T. M.-A.M. made the devices and measured the external quantum efficiencies with guidance from M.T. and M.C.-O. G.F.A.D. measured the current-voltage curves and performed optical simulations as well as electrical simulations with input from T.K. G.F.A.D. and T.K. measured the capacitance-voltage curves. S.E. measured the optical constants with guidance from H.H. and G.G. G.F.A.D., T.K., J.N. and J.R.D. wrote the paper. All authors commented on the manuscript and discussed the results. J.N. and J.R.D. initiated the project and guided and supervised the work.

## Additional information

Supplementary information accompanies this paper at <http://www.nature.com/scientificreports>

**Competing financial interests:** Merck Chemical is a world leader commercial enterprise engaged various R&D programs at different levels. The work reported here was carried out at both Merck facilities in Chilworth and UCSB; Merck is seeking to secure intellectual property rights on the polymers reported in this paper. G.F.A.D. was co-financed between Merck chemicals and the EPSRC, UK for the duration of this work in agreement with the CASE studentships award program from EPSRC, UK.

**How to cite this article:** Dibb, G.F.A. *et al.* Influence of doping on charge carrier collection in normal and inverted geometry polymer:fullerene solar cells. *Sci. Rep.* **3**, 3335; DOI:10.1038/srep03335 (2013).



This work is licensed under a Creative Commons Attribution 3.0 Unported license. To view a copy of this license, visit <http://creativecommons.org/licenses/by/3.0>